High-Performance UV–Visible–NIR Broad Spectral Photodetectors Based on One-Dimensional In2Te3 Nanostructures

ARTICLE *in* NANO LETTERS · AUGUST 2012

Impact Factor: 13.59 · DOI: 10.1021/nl302142g · Source: PubMed

4 AUTHORS, INCLUDING:

Muhammad Safdar
Bahauddin Zakariya University
39 PUBLICATIONS **609** CITATIONS
SEE PROFILE

Chao Jiang
National Center for Nanoscience and Technol…
70 PUBLICATIONS **407** CITATIONS
SEE PROFILE

Jun He
University of Western Australia
57 PUBLICATIONS **705** CITATIONS
SEE PROFILE

NANO LETTERS

Letter

pubs.acs.org/NanoLett

High-Performance UV−Visible−NIR Broad Spectral Photodetectors Based on One-Dimensional In_2Te_3 Nanostructures

Zhenxing Wang, Muhammad Safdar, Chao Jiang, and Jun He*

National Center for Nanoscience and Technology, Beijing 100190, P. R. China

Supporting Information

ABSTRACT: For the first time, high quality In_2Te_3 nanowires were synthesized via a chemical vapor deposition (CVD) method. The synthesized In_2Te_3 nanowires are single crystals grown along the [132] direction with a uniform diameter of around 150 nm and an average length of tens of micrometers. Further, two kinds of photodetectors made by 1D In_2Te_3 nanostructures synthesized by CVD and solvothermal (ST) methods respectively were fabricated. To our best knowledge, this is the first time photoresponse properties of In_2Te_3 nanowire have been studied. The CVD grown nanowire device shows better performance than the ST device, which demonstrates a fast, reversible, and stable photoresponse and also a broad light detection range from 350 nm to 1090 nm, covering the UV−visible−NIR region. The excellent performance of the In_2Te_3 nanowire photodetectors will enable significant advancements of the next-generation photodetection and photosensing applications.

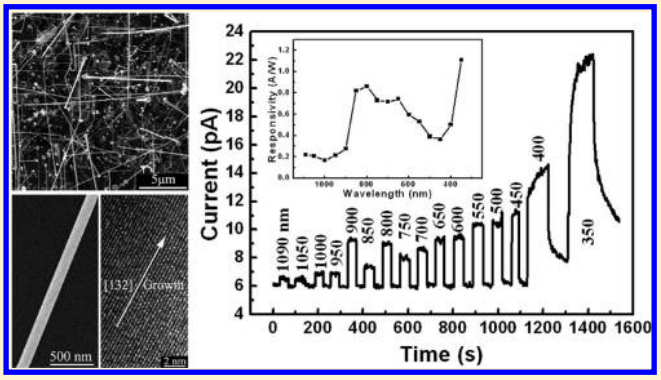

KEYWORDS: *Indium sesquitelluride, photodetector, broad spectra detection, UV−visible-NIR, chalcogenide*

Binary chalcogenide alloys $A_2^{III}B_3^{VI}$ (A = Al, Ga, In and B = S, Se, Te) have been largely investigated for the potential applications in energy conversion and information devices.[1−5] Indium sesquitelluride (In_2Te_3), an important III−VI compound semiconductor with a narrow direct bandgap of 1.19 eV at room temperature,[6] is a promising materials for applications in gas sensors,[7] memory devices,[8−10] and thermoelectric power generators.[11,12] However, previous research on In_2Te_3 devices is largely based on thin film, and no previous research has been reported on the synthesis and device application of In_2Te_3 nanowires. This is likely due to the great challenge of the In_2Te_3 nanowire synthesis.

Compared with thin film materials, the unique chemical and physical properties of semiconductor nanowire make it ideal for designing and developing advanced, functional nanodevices such as sensors, photodetectors, field-effect transistors, thermoelectronic power generators, and so forth.[13−26] Among them, photodetectors, which convert optical signals to electrical signals, are essential elements applied in high-resolution imaging technique, light wave communications, and optical interconnects.[18,19,27−30] Photodetectors based on various 1D semiconductor nanomaterials, such as ZnO,[31] CdS,[32] CdTe,[33,34] ZnS,[35] Zn_3P_2,[36] and so forth have been extensively investigated and show superior sensitivity and fast response speed. However, most of the research only studied the photoresponse performance under certain single wavelength light or the light with a narrow range. Moreover, some common types of photodetectors, such as GaN, Si, and InGaAs based detectors, can only detect the photo in a narrow spectral range.[37] Detecting ultraviolet (UV)-visible to near-infrared (NIR) is critical for varied scientific and industrial applications, so a photodetector with a broad spectral photoresponse is required.

Owing to high specific surface and confined quantum effect, 1D In_2Te_3 nanostructures have much improved chemical and physical properties compared with conventional thin film structures, especially in thermoelectric, topological insulators, sensing, and optoelectronic applications. With a similar crystal structure as In_2Te_3, indium selenide (In_2Se_3), the nanowire photodetector demonstrated high-performance, visible-light photoresponse properties.[38−40] Having a narrower bandgap, In_2Te_3 nanowire is expected to be suitable for photoresponse detection and potentially for wider spectral photodetectors.

In this paper, by optimizing the deposition parameters, we successfully demonstrate the synthesis of high-quality, single-crystalline In_2Te_3 nanowires with tens of micrometers in length and around 150 nm in diameter. To our best knowledge, this is the first report of the synthesis of single-crystalline In_2Te_3 nanowire via CVD. Further, two kinds of single In_2Te_3 nanowire photodetectors are fabricated. One is based on In_2Te_3 single-crystalline nanowire grown via the CVD method. The other one is based on single polycrystalline In_2Te_3 1D nanostructure synthesized via the solvothermal (ST) method. The photoresponse characteristics of the devices were systemically examined under the broad light range from 350 nm to 1090 nm. After comparing

Received: June 6, 2012
Revised: August 1, 2012
Published: August 21, 2012

   dx.doi.org/10.1021/nl302142g | *Nano Lett.* 2012, 12, 4715−4721

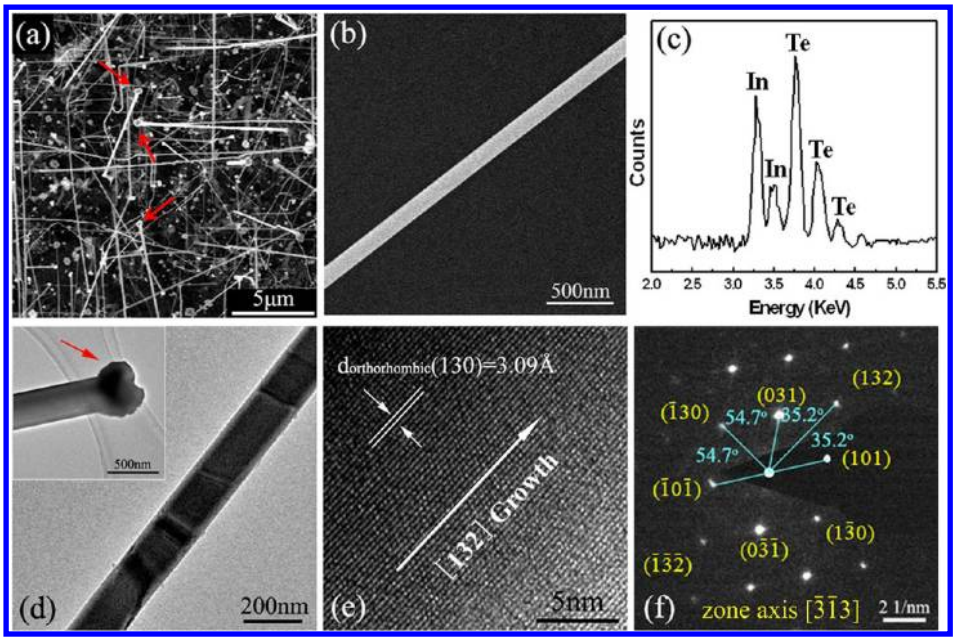

Figure 1. Characterization of as-grown In_2Te_3 nanowires by the CVD method. SEM images of (a) In_2Te_3 nanowires and (b) a typical single In_2Te_3 nanowire. (c) EDS spectrum of a single In_2Te_3 nanowire. (d) TEM and (e) HRTEM image of a single In_2Te_3 nanowire. TEM image of a typical metal-capped In_2Te_3 nanowire is shown in inset of d. (f) The corresponding selected area electron diffraction (SAED) pattern of the single In_2Te_3 nanowire in panel d. Note: For analysis convenience, two white spots (000) and (101), shaded by the tip, were artificially added into panel f.

the two photodetectors, the CVD-grown In_2Te_3 nanowire photodetector shows much better performance in this broad wavelength range. These results demonstrate that the CVD grown In_2Te_3 nanowires are promising candidates for applications in high sensitivity and high-speed nanoscale photodetectors with broad band photoresponse.

Figure 1a depicts an FESEM image of as-grown nanowires by CVD method, which reveals the formation of the nanowires with diameters mainly distributed in the 50−300 nm range. An SEM image with larger area indicates the nanowires are tens of micrometers in length and has high yield (Figure S1, in the Supporting Information). Metal nanoparticles can be explicitly seen at the top of the nanowires, indicated by red arrows in Figure 1a and in the inset of Figure 1d as well. This proves that the In_2Te_3 nanowire growth follows a vapor−liquid−solid (VLS) mechanism. It should be mentioned that no In_2Te_3 nanowire growth was observed on the same substrate when Au catalyst was not used. Further a magnified SEM image of a single In_2Te_3 nanowire is shown in Figure 1b. It is clear that the In_2Te_3 nanowire has a smooth surface and uniform diameter of around 135 nm along its entire length. An X-ray energy-dispersive spectrum (EDS) acquired from an individual nanowire exhibits strong In and Te peaks, and the atomic ratio is close to the 2:3 stoichiometry, as expected.

The perfect crystallinity of the In_2Te_3 nanowires was confirmed by the HRTEM and SAED patterns. The lattice planes (130) with the spacing distances of about 3.09 Å can be seen perpendicular to the growth direction, as shown in Figure 1e. Furthermore, the corresponding SAED pattern of single In_2Te_3 nanowire indicates its single crystalline microstructure, shown in Figure 1f. A series of *d*-spacings, 3.56 Å, 2.18 Å, and 3.09 Å according to the (101), (132), and (130) planes of In_2Te_3 with a body-centered structure of orthorhombic crystal system (JCPDS 89-3698), can be observed. It should be noted that the (031) plane has the same *d*-spacing with (101) plane. According to the orthorhombic crystal system, the angle between two planes has a relationship with the Miller index as follows:

$$\cos(\varphi) = \left(\frac{hh'}{a^2} + \frac{kk'}{b^2} + \frac{ll'}{c^2}\right) \Big/ \left(\sqrt{\frac{h^2}{a^2} + \frac{k^2}{b^2} + \frac{l^2}{c^2}} \times \sqrt{\frac{h'^2}{a'^2} + \frac{k'^2}{b'^2} + \frac{l'^2}{c'^2}}\right) \quad (1)$$

where φ is the angle between $(h\,k\,l)$ and $(h'\,k'\,l')$ planes and a, b, and c correspond to crystal cell parameters (a = 4.359 Å, b = 13.07 Å, and c = 6.165 Å). The angles 35.2° between (101) and (132) and 54.7° between (031) and (−130) were calculated and marked in Figure 1f. They are quite consistent with the angles measured in SAED pattern. Based on above analysis, it is further confirmed that the single crystalline In_2Te_3 nanowires synthesized by the CVD method grow along the [132] direction and belong to the orthorhombic crystal system.

To systematically investigate the performance of In_2Te_3 nanomaterial photodetectors, the solvothermal (ST) method was employed to synthesize 1D In_2Te_3 nanostructures besides the CVD method. The representative morphologies of the produced samples were investigated by FESEM. Figure 2a shows an FESEM image of a large number of produced 1D nanostructures with diameter from 100 nm to 1 μm. The length can approach several micrometers, even over tens of micrometers (Figure S2, in the Supporting Information). A typical single 1D nanostructure with a diameter about 1 μm is shown in Figure 2b. It is clear to see the surface is very rough and composed of many nanoparticles. The chemical composition of the 1D nanostructures was determined by the EDS spectrum. In and Te element signals have an approximate atomic ratio of In:Te = 2:3, shown in Figure 2c. A detailed microstructure of the In_2Te_3 1D nanostructures were further characterized by TEM and XRD. Consistent with the SEM image (Figure 2b), Figure 2d is a TEM image of single 1D nanostructure, which clearly reveals that

dx.doi.org/10.1021/nl302142g | *Nano Lett.* 2012, 12, 4715−4721

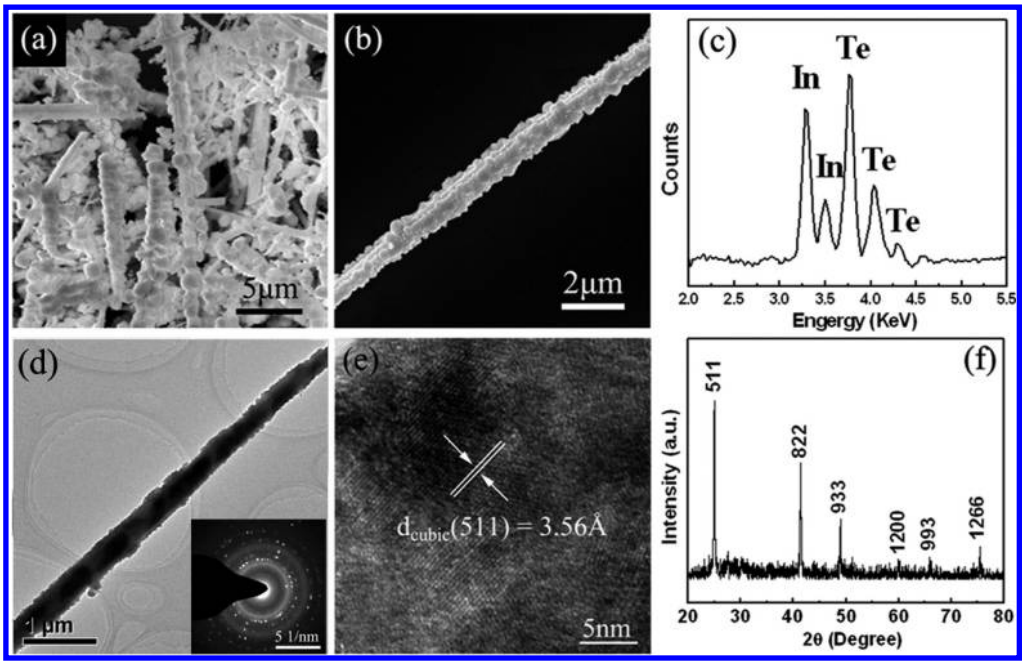

Figure 2. Characterization of as-synthesized 1D In_2Te_3 nanostructures by the solvothermal method. SEM images of (a) 1D In_2Te_3 nanostructures and (b) a typical single 1D nanostructure. (c) EDS pattern of a single 1D nanostructure. (d) TEM and (e) HRTEM image of In_2Te_3 nanostructure. Inset: SAED pattern of the In_2Te_3 nanostructure. (f) X-ray diffraction (XRD) patterns of as-synthesized samples.

the 1D nanostructure has a rough surface as well. SAED pattern with multirings demonstrates the polycrystalline nature of the 1D nanostructure, as shown in the inset of Figure 2d. In Figure 2f, the XRD pattern exhibits three strong peaks at $2\theta = 25.0°$, 41.4°, and 49.0°, which are assigned to diffractions of the (511), (822), and (933) planes, respectively. In addition, three weak peaks at $2\theta = 60.0°$, 66.0°, and 75.5° accord to (1200), (993) and (1266) planes, respectively. The XRD pattern proves the face-centered structure of the 1D nanostructure with lattice constant of $a = b = c = 18.48$ Å (JCPDS 33-1488). The plane with the d-spacing of 3.56 Å was also observed in the HRTEM image shown in Figure 2e, according to (511) plane.

Two kinds of devices were fabricated on silicon substrates with a 300 nm thick thermal oxide layer using 1D In_2Te_3 nanostructures, synthesized by CVD and ST methods, respectively. We refer to these as CVD device and ST device for convenience. SEM images of the both device structures are shown in insets of Figure 3a and e. The electrical properties were measured using a traditional two-probe method. Photoresponse characteristics under a 633 nm laser (Melles Griot) with the intensity of 47.8 mW/cm^2 are shown in Figure 3a–d for the CVD device and Figure 3e–h for the ST device.

Figure 3a,e shows typical current versus voltage curves of CVD and ST photodetectors in the dark and under laser illumination. Gold was used as contacts in our devices. A little nonlinearity of the I–V curves should be relative to the mismatch work function between In_2Te_3 and gold. The drastic increase in current under laser illumination is observed compared to the current in the dark. It is worth noting that the CVD device has a lower dark current than the ST device, which could be attributed to their different morphologies. The In_2Te_3 nanowire of the CVD device has a diameter about 138 nm, far less than 1.08 μm of the ST device, which brings the lower conductivity of CVD device. Figure 3b,f displays the time photoresponse of the both photodetectors with the laser switched on and off at a fixed voltage of 10 V. The "on" and "off" states for eight cycles keep the same current level, respectively, indicating the excellent reversibility and stability of 1D In_2Te_3 nanostructure photodetectors. Furthermore, the analysis from an enlarged photoresponse process containing one rise and one reset (Figure 3c,f) shows both devices have fast detection times. The rising and reset time of these two devices are faster than 70 ms. This is faster than that of most other photodetectors[31,33−35,41] and even than that of In_2Se_3 nanowire photodetectors.[39,40] It should be mentioned that 70 ms is the present experimental setup limits. The on/off ratio is ∼33 and 4.2 for CVD and ST devices, respectively. The higher on/off ratio of CVD device is ascribed to its high surface-to-volume ratio, high crystal quality, and relevant lower dark current.

The detector current responsivity (R_λ) and the external quantum efficiency (EQE) are both critical parameters for photodetectors, which determine the photodetector sensitivity. R_λ is defined as the photocurrent generated per unit power of incident light on the effective area of a photodetector.[39] EQE is defined as the number of electrons detected per incident photon. R_λ and EQE can be calculated in the following equations:[40]

$$R_\lambda = \Delta I_\lambda/(P_\lambda S) \tag{2}$$

$$\mathrm{EQE} = hcR_\lambda/(e\lambda) \tag{3}$$

where $\Delta I_\lambda = I_\lambda - I_{dark}$ is the photocurrent, P_λ is the incident light intensity, S is the effective illuminated area, h is Planck's constant, c is the light velocity, e is the electronic charge, and λ is the incident light wavelength. For CVD device, $\Delta I_\lambda = 196$ pA, $P_\lambda = 47.8$ mW/cm^2, $S = \sim 1.5$ μm^2, $\lambda = 633$ nm, then R_λ(CVD) and EQE(CVD) can be estimated to be about 0.3 A/W and 0.6, respectively. For ST device, $\Delta I_\lambda = 129$ pA, $P_\lambda = 47.8$ mW/cm^2, $S = \sim 20.3$ μm^2, $\lambda = 633$ nm, then R_λ(ST) and EQE(ST) can be calculated to be about 0.013 A/W and 0.026, respectively. The photoresponse characteristics of the two photodetectors are summarized in Table 1. Obviously, the CVD photodetector has higher performance than ST device. Xie et al.[33] reported that the device configuration had a drastic influence on the sensitivity of

dx.doi.org/10.1021/nl302142g | Nano Lett. 2012, 12, 4715−4721

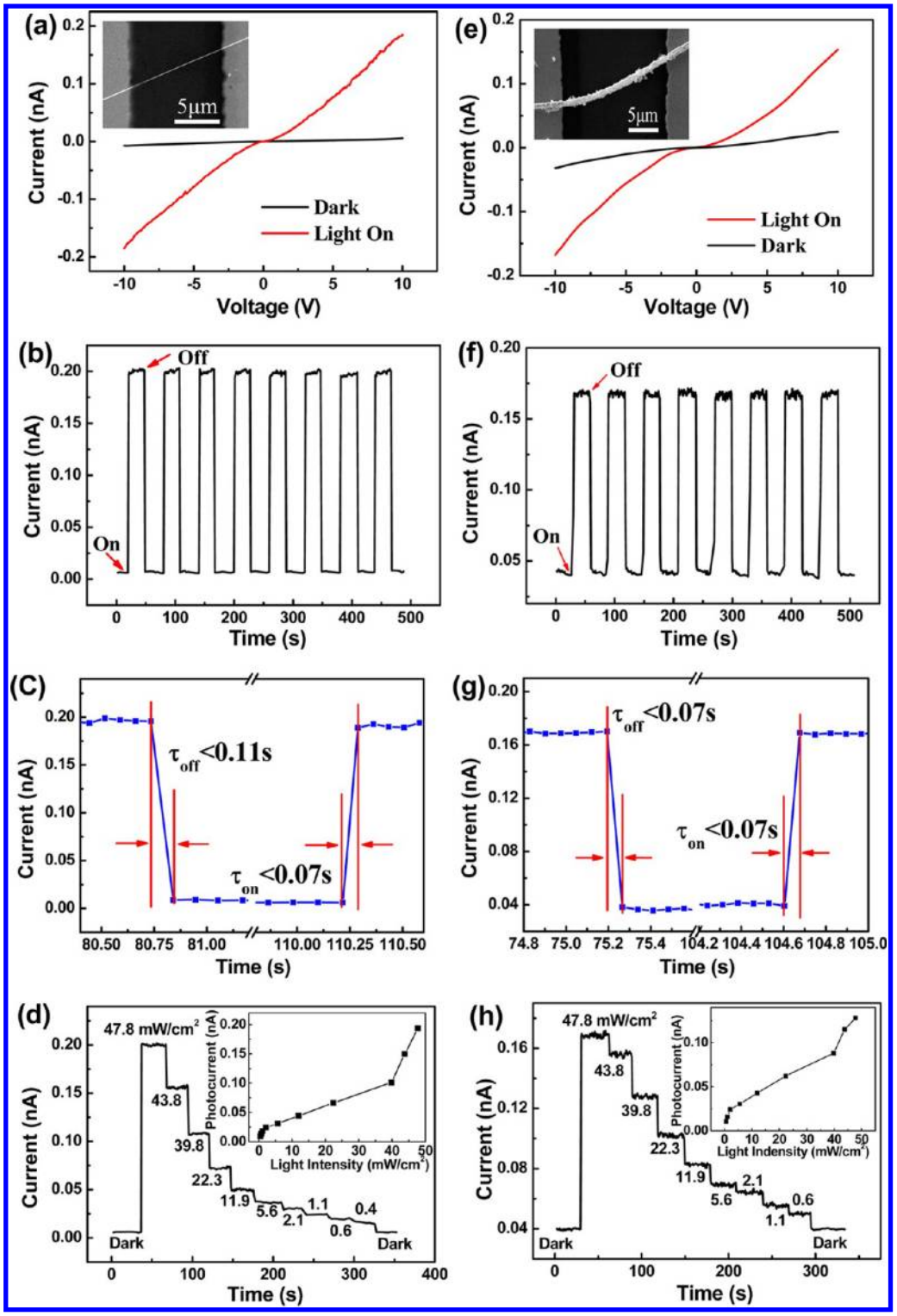

Figure 3. Photoresponse characteristics of a single In_2Te_3 nanowire device, grown by the CVD method shown in panels a–d, and a single 1D nanostructure device, synthesized by the ST method shown in panels e–h. (a, e) *I*–*V* curves of both devices under dark condition and while illuminated by a laser with 633 nm wavelength and 47.8mW/cm^2 power intensity. (b, f) Time-dependent photocurrent response of the both devices with the laser on and off at the voltage of 10 V. (c, g) Enlarged portions of one response and reset process. (d, h) Photocurrent under the light with different power at same bias of 10 V. Insets: photocurrent vs incident light intensity of both devices at a bias of 10 V.

photodetectors, especially the channel length. They found that a shorter channel and larger surface-to-volume ratio would yield higher R_λ and EQE. In our case, the In_2Te_3 nanowires grown by the CVD method have a higher surface-to-volume ratio than 1D nanostructure synthesized by the ST method. This enables the CVD device to have higher performance. Meanwhile, we believe the R_λ and EQE can be significantly increased by improving the device configuration.

The relationship between the photocurrent and the light intensity was also investigated. Figure 3d,h shows the photocurrent

dx.doi.org/10.1021/nl302142g | *Nano Lett.* 2012, 12, 4715–4721

step-like decreases as the light intensity is reduced. The photocurrent is linearly proportional to the incident irradiation intensity within the range of ~2−40 mW/cm^2, shown in both insets of Figure 3d and h. Within the linear range, the In_2Te_3 nanostructure should be a typical photon-dependent resistor; that is, the more photons will generate more electron−hole pairs.[40] We have another CVD device to give the similar linear zone (Figure S3, in the Supporting Information). However, it is still not clear why the photocurrent is nonlinear with light intensity beyond the linear range. A deeper investigation will be required to study the mechanism.

Broad spectral detection is beneficial for extending the application range of photodetectors. The photoresponse characteristics of both CVD and ST devices were investigated under three typical given lights 830, 550, and 350 nm crossing over the UV−visible−NIR range, as shown in Figure 4a−c for the CVD device and Figure 4d−f for the ST device. Both CVD and ST photodetectors demonstrate fast, reversible, and stable photoresponse properties under 830 and 550 nm light by switching the lights on and off alternatively. However, lower noise in Figure 4a,b for the CVD device than in Figure 4d,e for the ST device is observed. This signifies that the CVD device can detect a lower limit of light power. Compared with the 830 and 550 nm light, the photoresponse characteristics under 350 nm have two evident features. One is that the response and reset times become longer, and the other is that the baseline shifts to a higher current level. We confer that these phenomena probably originate from absorption and desorption process of gas molecules on the In_2Te_3 surface under higher energy UV light, which will not be caused by visible and NIR light with lower energy.[28,31] In addition, various traps in the nanowires can also affect the response and reset time.[33,42] These traps were involved in the photoresponse precesses of In_2Te_3 nanowires under UV light illumination and thus deteriorate the response speed performance of In_2Te_3 photodetector. In other hand, these traps decrease the electron−hole recombination, thus prolonging the lifetime of

Table 1. Characteristics of ST and CVD Photodetectors

device type	dark current (pA)	on/off ratio	responsivity (AW^{-1})	EQE
CVD	~6@10 V	33	~0.3	~0.6
ST	~41@10 V	4.2	~0.013	~0.026

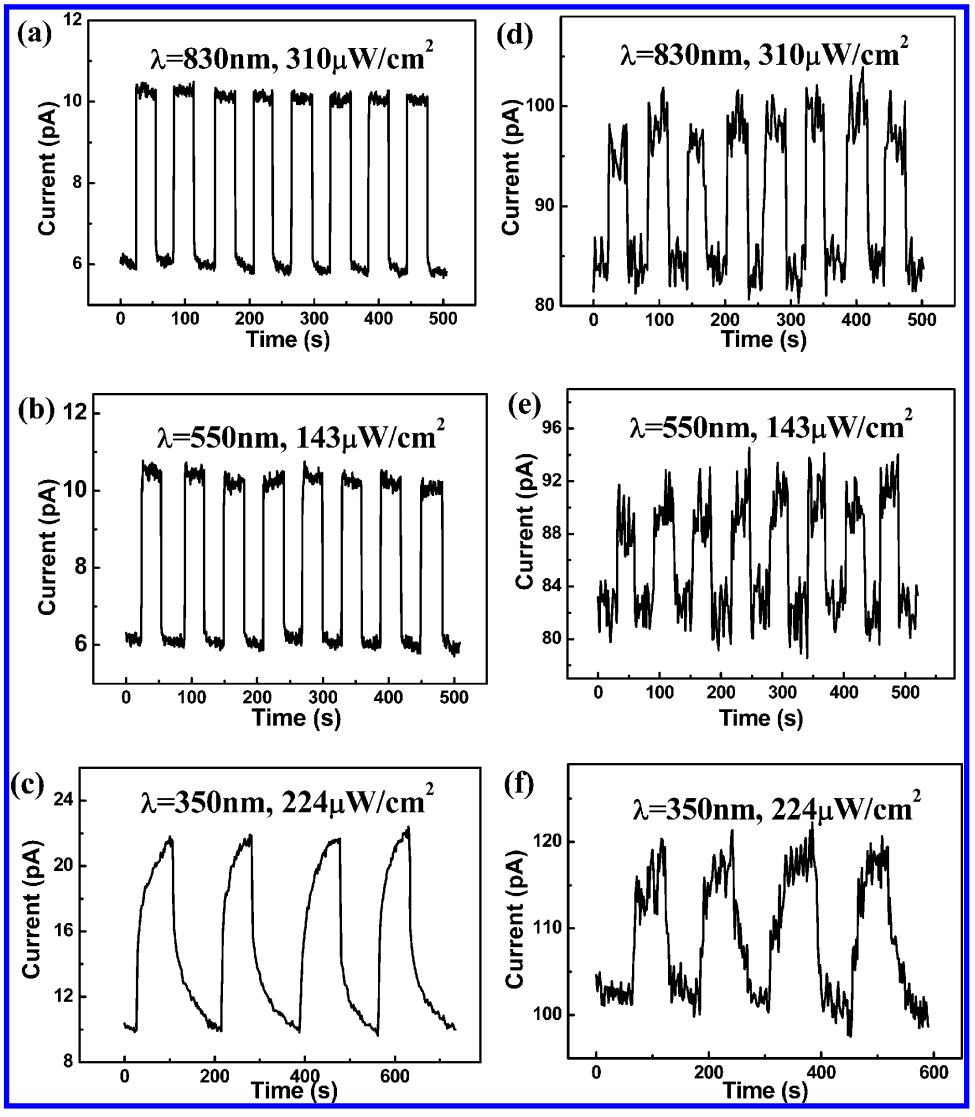

Figure 4. Photoresponse of the CVD device (a, b, and c) and the ST device (d, e, and f) illuminated under 830 nm, 550 nm, and 350 nm, respectively, by switching the light on and off at a 10 V bias.

dx.doi.org/10.1021/nl302142g | *Nano Lett.* 2012, 12, 4715−4721

carriers, which will enhance the responsivity of the device. This point is confirmed in the inset of Figure 5, as larger responsivity

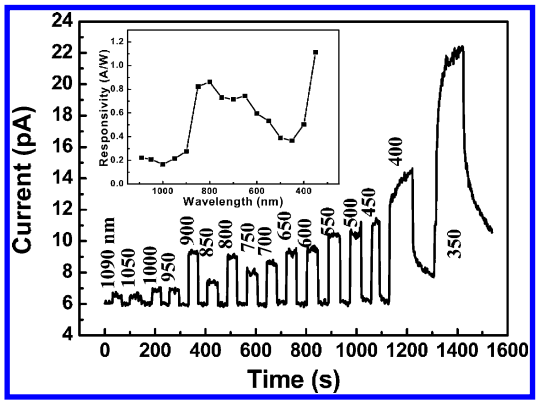

Figure 5. Photoresponse characteristics of CVD device under different wavelength light illumination at 10 V bias. Inset: current responsivity under different wavelength light illumination.

under UV illumination. Further, the photoresponse characteristics of the CVD device under the light within a large range from 350 nm to 1090 nm were investigated, shown in Figure 5. It clearly shows that a single In_2Te_3 nanowire photodetector has broad spectral detection range from UV−visible to NIR.

In conclusion, 1D In_2Te_3 nanostructures were synthesized by the CVD and ST methods. We believe that this is the first time high quality In_2Te_3 nanowires are synthesized by the CVD method. The synthesized In_2Te_3 nanowires are single crystals grown along the [132] direction with a uniform diameter of around 150 nm and a typical length of tens of micrometers. Furthermore, two kinds of photodetectors, CVD and ST devices, were fabricated to study photoresponse properties of In_2Te_3 nanomaterials. The CVD device shows better performance than the ST device, which demonstrates a fast, reversible, and stable photoresponse and also has a broad light detection range from 350 nm to 1090 nm, covering the UV−visible−NIR region. The excellent performance of the In_2Te_3 nanowire photodetectors will enable significant advancements of the next generation of photodetection and photosensing applications.

Methods. *Synthesis of In_2Te_3 Nanostructure by the Solvothermal Method.* Sodium telluride Na_2TeO_3 (0.3 g) and indium hydrated $In(NO_3)_2{\cdot}5H_2O$ (0.35 g) were slowly added in an alkaline solvent ethylene glycol in a beaker and stirred for 30 min at room temperature. Then EDA 2.2 mL and EG 30 mL were carefully added into the solution, which sequentially changed from milky white to colorless. The pH value was adjusted with ammonia to maintain a balance between 9 and 10. The 30 mL of final clear solution was transferred into the Teflon vessel, and the container was closed and maintained at 200 °C for 24 h. After that the autoclave was cooled to room temperature naturally, and the final product in black-gray color was centrifuged and washed several times with double-distilled water and absolute ethanol and dried in a vacuum at 60 °C for 8 h.

Synthesis of In_2Te_3 1D Nanostructure by the CVD Method. In_2Te_3 powder (99.999%) was used for synthesis of single crystalline indium telluride nanowires in a tube furnace via a chemical vapor deposition method. The synthesis was carried out using Si (100) wafer substrate deposited with 10 nm gold catalyst thin film and pure Ar mixed with 50% H_2 were used as the carrier gases. The flow rate of 10−25 SCCM and pressure of 100−250 Torr was used. In_2Te_3 powder placed at the center of the quartz tube at 700−850 °C as the source and substrate was loaded downstream at 550−650 °C, as the target and furnace temperature was maintained for 60−90 min for the growth period.

Characterization of As-Synthesized Samples. The morphology, composition, and microstructures of the synthesized products were characterized by a field emission scanning electron microscope (FESEM, Hitachi S-4800) and a high resolution transmission electron microscope (HRTEM, FEI F20) equipped with an X-ray energy dispersive spectrometer (EDS). The microstructures were also measured by X-ray diffraction (XRD, D/Max-TTRIII(CBO) diffractometer) using Cu Kα radiation (λ = 1.5418 Å).

Fabrication and Measurements of Single In_2Te_3 Nanowire Devices. To fabricate single-nanowire devices, the In_2Te_3 nanowires were released into ethanol by sonication of growth substrates. The nanowires were further dispersed onto silicon wafers with a 300 nm thick thermal oxide layer. The electrical contacts to individual In_2Te_3 nanowire were defined by copper grid shadow mask with the typical gaps of 15 or 20 μm, and subsequently 8 nm Cr and 100 nm Au was evaporated, respectively. The transport characteristics of these devices were measured at room temperature in the ambient air using an Everbeing manual probe station equipped with a Keithley 4200 semiconductor characterization system. To initiate the photocurrent, we measured DC photoconductivity at room temperature in ambient air by illuminating the devices using a relative light source.

■ ASSOCIATED CONTENT

Supporting Information

Figures S1−S3: SEM and optical images of the nanowires and a photocurrent vs light intensity plot. This material is available free of charge via the Internet at http://pubs.acs.org.

■ AUTHOR INFORMATION

Corresponding Author

*E-mail: hej@nanoctr.cn.

Notes

The authors declare no competing financial interest.

■ ACKNOWLEDGMENTS

This work at National Center for Nanoscience and Technology was supported by 973 Program of the Ministry of Science and Technology of China (No. 2012CB934103) and the 100-Talents Program of the Chinese Academy of Sciences (No. Y1172911ZX).

■ REFERENCES

(1) Rhyee, J. S.; Lee, K. H.; Lee, S. M.; Cho, E.; Kim, S., II; Lee, E.; Kwon, Y. S.; Shim, J. H.; Kotliar, G. *Nature* **2009**, *459*, 965.
(2) Strothkämper, C.; Schwarzburg, K.; Schütz, R.; Eichberger, R.; Bartelt, A. *J. Phys. Chem. C* **2012**, *116*, 1165.
(3) Ohta, T.; Schmidt, D. A.; Meng, S.; Klust, A.; Bostwick, A.; Yu, Q.; Olmstead, M. A.; Ohuchi, F. S. *Phys. Rev. Lett.* **2005**, *94*, 116102.
(4) Kurosaki, K.; Matsumoto, H.; Charoenphakdee, A.; Yamanaka, S.; Ishimaru, M.; Hirotsu, Y. *Appl. Phys. Lett.* **2008**, *93*, 012101.
(5) Park, K. H.; Jang, K.; Son, S. U. *Angew. Chem. Int. Ed.* **2006**, *45*, 4608.
(6) Golding, T. D.; Boyd, P. R.; Martinka, M.; Amirtharaj, P. M.; Dnan, J. H. *J. Appl. Phys.* **1989**, *65*, 1936.
(7) Desai, R. R.; Lakshminarayana, D.; Patel, P. B.; Panchal, C. J. *Sens. Actuators, B* **2005**, *107*, 523.
(8) Zhu, H.; Chen, K.; Ge, Z. Y.; Xu, H. N.; Su, Y.; Yin, J.; Xia, Y. D.; Liu, Z. G. *J. Mater. Sci.* **2010**, *45*, 3569.
(9) Afifi, M. A.; Hegab, N. A.; Bakheet, A. E. *Vacuum* **1996**, *47*, 265.

(10) Balevicius, S.; Cesnys, A.; Deksnys, A. *Phys. Status Solidi A* **1975**, *32*, K41.
(11) Lakshminarayana, D.; Patel, P. B.; Desai, R. R.; Panchal, C. J. *J. Mater. Sci. Mater. Electron.* **2002**, *13*, 27.
(12) Tai, G. A.; Miao, C. Y.; Wang, Y. B.; Bai, Y. R.; Zhang, H. Q.; Guo, W. L. *Nanoscale Res. Lett.* **2011**, *6*, 329.
(13) Xia, Y. N.; Yang, P. D.; Sun, Y. G.; Wu, Y. Y.; Mayers, B.; Gates, B.; Yin, Y. D.; Kim, F.; Yan, H. Q. *Adv. Mater.* **2003**, *15*, 353.
(14) Pan, Z. W.; Dai, Z. R.; Wang, Z. L. *Science* **2001**, *291*, 1947.
(15) Huang, Y.; Duan, X. F.; Lieber, C. M. *Small* **2005**, *1*, 142.
(16) Huang, M. H.; Mao, S.; Feick, H.; Yan, H. Q.; Wu, Y. Y.; Kind, H.; Weber, E.; Russo, R.; Yang, P. D. *Science* **2001**, *292*, 1897.
(17) Duan, X. F.; Huang, Y.; Agarwal, R.; Lieber, C. M. *Nature* **2003**, *421*, 241.
(18) Jie, J. S.; Zhang, W. J.; Jiang, Y.; Meng, X. M.; Li, Y. Q.; Lee, S. T. *Nano Lett.* **2006**, *6*, 1887.
(19) Fan, Z. Y.; Ho, J. C.; Jacobson, Z. A.; Razavi, H.; Javey, A. *Proc.Natl. Acad. Sci. U.S.A.* **2008**, *105*, 11066.
(20) Shen, G. Z.; Xu, J.; Wang, X. F.; Huang, H. T.; Chen, D. *Adv. Mater.* **2011**, *23*, 771.
(21) Majumdar, A.; Chen, R.; Hochbaum, A. I.; Murphy, P.; Moore, J.; Yang, P. D. *Phys. Rev. Lett.* **2008**, *101*, 105501.
(22) Chen, D.; Xu, J.; Liang, B.; Wang, X. F.; Chen, P. C.; Zhou, C. W.; Shen, G. Z. *J. Mater. Chem.* **2011**, *21*, 1723.
(23) Das, S.; Yan, H.; Choe, H. S.; Nam, S. W.; Hu, Y. J.; Klemic, J. F.; Ellenbogen, J. C.; Lieber, C. M. *Nature* **2011**, *470*, 240.
(24) Hu, Y. F.; Zhou, J.; Yeh, P. H.; Li, Z.; Wei, T. Y.; Wang, Z. L. *Adv. Mater.* **2010**, *22*, 3327.
(25) Li, L.; Lee, P. S.; Yan, C. Y.; Zhai, T. Y.; Fang, X. S.; Liao, M. Y.; Koide, Y.; Bando, Y.; Golberg, D. *Adv. Mater.* **2010**, *22*, 5145.
(26) Zhai, T. Y.; Li, L.; Ma, Y.; Liao, M. Y.; Wang, X.; Fang, X. S.; Yao, J. N.; Bando, Y.; Golberg, D. *Chem. Soc. Rev.* **2011**, *40*, 2986.
(27) Wang, J.; Gudiksen, M. S.; Duan, X.; Cui, Y.; Lieber, C. *Science* **2001**, *293*, 1455.
(28) Kind, H.; Yan, H. Q.; Messer, B.; Law, M.; Yang, P. D. *Adv. Mater.* **2002**, *14*, 158.
(29) Soci, C.; Zhang, A.; Xiang, B.; Dayeh, S. A.; Aplin, D. P. R.; Park, J.; Bao, X. Y.; Lo, Y. H.; Wang, D. *Nano Lett.* **2007**, *7*, 1003.
(30) Wang, J. J.; Cao, F. F.; Jiang, L.; Guo, Y. G.; Hu, W. P.; Wan, L. J. *J. Am. Chem. Soc.* **2009**, *131*, 15602.
(31) Zhou, J.; Gu, Y. D.; Hu, Y. F.; Mai, W. J.; Yeh, P. H.; Bao, G.; Sood, A. K.; Polla, D. L.; Wang, Z. L. *Appl. Phys. Lett.* **2009**, *94*, 191103.
(32) Ye, Y.; Dai, L.; Wen, X. N.; Wu, P. C.; Pen, R. M.; Qin, G. G. *ACS Appl. Mater. Interfaces* **2010**, *10*, 2724.
(33) Xie, X.; Kwok, S. Y.; Lu, Z. Z.; Liu, Y. K.; Cao, Y. L.; Luo, L. B.; Zapien, J. A.; Bello, I.; Lee, C. S.; Lee, S. T.; Zhang, W. J. *Nanoscale* **2012**, *4*, 2914.
(34) Ye, Y.; Sun, T.; You, L. P.; Zhu, R.; Gao, J. Y.; Peng, R. M.; Yu, D. P.; Qin, G. G. *Appl. Phys. Lett.* **2010**, *108*, 044301.
(35) Wang, X. F.; Xie, Z.; Huang, H. T.; Liu, Z.; Chen, D.; Shen, G. Z. *J. Mater. Chem.* **2012**, *22*, 6845.
(36) Wu, P. C.; Dai, Y.; Ye, Y.; Yin, Y.; Dai, L. *J. Mater. Chem.* **2011**, *21*, 2563.
(37) Gong, X.; Tong, M. H.; Xia, Y. J.; Cai, W. Z.; Moon, J. S.; Cao, Y.; Yu, G.; Shieh, C. L.; Nilsson, B.; Heeger, A. J. *Science* **2009**, *325*, 1665.
(38) Wang, J. J.; Cao, F. F.; Jiang, L.; Guo, Y. G.; Hu, W. P.; Wan, L. J. *J. Am. Chem. Soc.* **2009**, *131*, 15602.
(39) Zhai, T. Y.; Fang, X. S.; Liao, M. Y.; Xu, X. J.; Li, L.; Liu, B. D.; Koide, Y.; Ma, Y.; Yao, J. N.; Bando, Y.; Golberg, D. *ACS Nano* **2010**, *4*, 1596.
(40) Li, Q. L.; Li, Y.; Gao, J.; Wang, S. D.; Sun, X. H. *Appl. Phys. Lett.* **2011**, *99*, 243105.
(41) Wang, Z. X.; Zhan, X. Y.; Wang, Y. J.; Muhammad, S.; Huang, Y.; He, J. *Nanoscale* **2012**, *4*, 2678.
(42) Jiang, Y.; Zhang, W. J.; Jie, J. S.; Meng, X. M.; Fan, X.; Lee, S. T. *Adv. Funct. Mater.* **2007**, *17*, 1995.